Editors' Suggestion

Pure quartic three-dimensional spatiotemporal Kerr solitons in graded-index media

Pedro Parra-Rivas,[1,*] Yifan Sun,[1] Fabio Mangini,[1] Mario Ferraro,[1] Mario Zitelli,[1] and Stefan Wabnitz[1,2]

[1]*Dipartimento di Ingegneria dell'Informazione, Elettronica e Telecomunicazioni, Sapienza Universitá di Roma, via Eudossiana 18, 00184 Rome, Italy*

[2]*INO, Istituto Nazionale di Ottica, Via Campi Flegrei 34, 80078 Pozzuoli, Italy*

(Received 31 October 2023; accepted 7 February 2024; published 15 March 2024)

We analyze the formation of three-dimensional spatiotemporal solitons in waveguides with a parabolic refractive index profile and pure quartic chromatic dispersion. We show, by applying both variational approaches and full three-dimensional numerical simulations, that fourth-order dispersion has a positive impact on soliton stabilization against spatiotemporal wave collapse. Specifically, pure quartic spatiotemporal solitons remain stable within a significantly larger energy range with respect to their second-order dispersion counterparts.

DOI: 10.1103/PhysRevA.109.033516

I. INTRODUCTION

The formation of high-dimensional solitons is a very intense field of research in different domains of science, ranging from nonlinear optics to Bose-Einstein condensates (BECs) [1–3]. In nonlinear optics, the formation of three-dimensional spatiotemporal solitons (STS), also known as *light bullets* [4], has been predicted in Kerr nonlinear lossless materials. Their formation is based on the counterbalance between the action of the intensity-dependent refractive index on the one hand and the combined effect of dispersion and diffraction on the other hand [1]. One of the main properties of these nonlinear waves is that, once they form, they can propagate indefinitely, without any shape modification. However, in experiments, the STSs have only been generated as transient objects, owing to instabilities associated with the presence of high-order effects [5–7].

In Kerr media, the most common instability is *spatiotemporal wave collapse*, whereby the strong contraction of a nonlinear wave leads to a catastrophic blow-up of its amplitude after a finite propagation distance [4,8,9]. Many different mechanisms have been proposed for STS stabilization, including saturable absorption, nonlocal and quadratic nonlinearities, and photonic lattices, to cite a few [2,3,9,10]. The positive impact of dissipative terms on the stabilization of STS has been also extensively studied in active cavities (see, for example, Refs. [2,3,11,12] and references therein), and very recently in passive ones [13]. Another stabilization mechanism relies on a parabolic modification of the transverse refractive index profile of the material, as it occurs in graded index (GRIN) multimode waveguides or fibers [14].

The parabolic index profile acts as a trapping potential, which is able to arrest the wave collapse, as predicted by Yu *et al.* [15] and Raghavan *et al.* [16] by means of variational approaches. For low pulse energy regimes, these results are well confirmed by full three-dimensional (3D) numerical solutions of the nonlinear wave equation. However, for sufficiently high pulse energies, even below the theoretically predicted instability threshold, this mechanism fails to arrest the collapse [17]. Thus, one may wonder if there are other alternatives for enlarging the energy-dependent stability range of light bullets.

The use of high-order dispersive effects has proved key for stabilizing temporal solitons in nonlinear cavities: Specifically, consider the case of third- [18–20] or fourth-order dispersion [21]. Moreover, the effect of pure quartic dispersion in soliton formation has been studied in the context of microcomb generation [22,23], mode-locked lasers [24], and single-pass (conservative) systems, where pure quartic solitons have been theoretically studied [25–28] and experimentally demonstrated [29–31]. Pure quartic temporal solitons possess flatter spectra and favorable energy scaling with pulse duration, which makes them particularly attractive from the point of view of applications. Moreover, the combination of anomalous quadratic and negative quartic dispersion is able to stabilize light bullets in homogeneous planar waveguides and bulk media [32,33].

In this article, we demonstrate theoretically the existence of time-symmetric (i.e., t-symmetric) positive pure quartic STSs in GRIN waveguides. To do so, we neglect second-order or quadratic dispersion, as well as odd-orders of dispersion (e.g., third-order) which otherwise would break such a symmetry. In this regard, one of the most remarkable results that we obtain is that pure quartic dispersion alone is able to significantly suppress wave collapse, thus greatly favoring STS stability. To perform this analysis, we follow a twofold approach, based on both the Ritz optimization method (i.e., the variational approach) [34,35] and direct full 3D numerical simulations.

We need to mention that in the presence of GRIN inhomogeneities, the spatiotemporal localization of light can be also interpreted as a nonlinear deformation of the fundamental Laguerre-Gaussian mode associated with the linear system [36], and therefore may lead to discrepancies about the correctness of refereeing to such a state as soliton. However, based on our work [17,37], and following previous literature [1,2,6,16], we have decided, for consistency, to use the term soliton, in particular STS, to refer to these states.

*pedro.parra-rivas@uniroma1.it

This article is organized as follows. In Sec. II we introduce the mathematical model that we will use. In Sec. III we apply, following a variational approach, the Ritz optimization method to compute approximate analytical STS solutions and to predict their stability. Section IV is devoted to comparing the analytical findings with full 3D numerical simulations. Finally, in Sec. V we summarize our work, drawing some final conclusions.

II. THE MODEL

In the paraxial and slowly varying envelope approximations, and neglecting the modal dispersion, the complex amplitude of the electric field E propagating in waveguides with a GRIN profile at the carrier frequency ω_0 can be described by the Gross-Pitaevskii equation with a two-dimensional (2D) parabolic potential [16]

$$\partial_Z E = \frac{i}{2\beta_0}\nabla_\perp^2 E + i\frac{\beta_4}{4!}\partial_T^4 E + in_1 k_0 R^2 E + ik_0 n_2 |E|^2 E, \quad (1)$$

where $k_0 = \omega_0/c$, $\beta_0 = n_0(\omega_0)k_0$, $\beta_4 = d^4\beta/d\omega^4|_{\omega_0}$, and $\beta(\omega) = n_0(\omega)\omega/c$, with $n_0(\omega)$ being the homogeneous contribution of the refractive index. $\nabla_\perp^2 \equiv \partial_X^2 + \partial_Y^2$ represents diffraction, the ∂_T^4 term results from fourth-order chromatic dispersion with T being the time variable, n_1 governs the parabolic variation $R^2 \equiv X^2 + Y^2$ of the refractive index in the transverse dimensions X and Y, and n_2 is the refractive index nonlinear coefficient responsible for the self-focusing or self-defocusing Kerr nonlinearity [1,14]. By taking the scaling transformations

$$E = e_c u, \quad T = t_c t, \quad (X, Y) = w_c(x, y), \quad Z = z_c z,$$

with

$$e_c^4 \equiv \frac{2}{k_0\beta_0}\frac{|n_1|}{|n_2|^2}, \qquad t_c^4 \equiv \frac{|\beta_4|}{4!}\sqrt{\frac{\beta_0}{2k_0|n_1|}},$$

$$w_c^4 \equiv \frac{1}{2k_0\beta_0|n_1|}, \qquad z_c^2 \equiv \frac{\beta_0}{2k_0|n_1|},$$

Eq. (1) becomes

$$\partial_z u = \frac{i}{2}\nabla_\perp^2 u + id_4\partial_t^4 u + i\frac{\rho}{2}(x^2 + y^2)u + i\nu|u|^2 u, \quad (2)$$

with $d_4 = \text{sign}(\beta_4) = \pm 1$, $\nu = \text{sign}(n_2) = \pm 1$ for self-focusing and self-defocusing nonlinearity, and $\rho = \text{sign}(n_1) = \pm 1$ for antiguiding and guiding materials, respectively. In an optical context, Eq. (1) is also referred to as a nonlinear Schrödinger equation with a 2D parabolic potential [1].

III. VARIATIONAL APPROACH

The Lagrangian density associated with Eq. (2) reads

$$\mathcal{L} = -\frac{1}{2}(|u_x|^2 + |u_y|^2) - d_4|u_{tt}|^2 + \frac{\rho}{2}(x^2 + y^2)|u|^2 + \frac{\nu}{2}|u|^4 + \frac{i}{2}(u^* u_z - uu_z^*), \quad (3)$$

and by defining the generalized field momenta $\mathcal{P} \equiv \partial_{u_z^*}\mathcal{L} = -iu/2$ and $\mathcal{P}^* \equiv \partial_{u_z}\mathcal{L} = iu^*/2$, we can obtain the Hamiltonian density $\mathcal{H}$ through the Legendre transform $\mathcal{H} = \mathcal{P}u_z^* + \mathcal{P}^* u_z - \mathcal{L}$ [38]. Here, we focus on shape-preserving and vorticity-free solitons. Therefore, we write $u(x, y, z, t) = v(x, y, t)e^{i\kappa z}$, where κ is the propagation constant (or chemical potential in the context of BECs) [1], and $v(x, y, t)$ is a real-valued function, describing the steady-state field. With this transformation, the Lagrangian density becomes

$$\mathcal{L}_v = -\frac{1}{2}(v_x^2 + v_y^2) - d_4 v_{tt}^2 + \frac{\rho}{2}(x^2 + y^2)v^2 + \frac{\nu}{2}v^4 - \kappa v^2. \quad (4)$$

Using the Legendre transform previously introduced and the transformation $u(x, y, z, t) = v(x, y, t)e^{i\kappa z}$, the Hamiltonian density reads

$$\mathcal{H} = \frac{1}{2}(v_x^2 + v_y^2) + d_4 v_{tt}^2 - \frac{\nu}{2}v^4 - \frac{\rho}{2}(x^2 + y^2)v^2. \quad (5)$$

The z-independent Euler-Lagrange equations

$$\frac{d^2}{dt^2}\left(\frac{\partial\mathcal{L}_v}{\partial v_{tt}}\right) + \frac{d}{dx}\left(\frac{\partial\mathcal{L}_v}{\partial v_x}\right) + \frac{d}{dy}\left(\frac{\partial\mathcal{L}_v}{\partial v_y}\right) - \frac{\partial\mathcal{L}_v}{\partial v} = 0 \quad (6)$$

lead to the steady-state partial differential equation

$$\frac{1}{2}\nabla_\perp^2 v + d_4\partial_t^4 v + \frac{\rho}{2}(x^2 + y^2)v + \nu v^3 - \kappa v = 0. \quad (7)$$

Note that Eq. (7) can also be obtained by a direct substitution of $u(x, y, z, t) = v(x, y, t)e^{i\kappa z}$ into Eq. (2).

In what follows, by applying the Ritz optimization method [34,35], we will compute an approximate analytical steady STS solution of Eq. (7). This method relies on the proper selection of a trial function, or solution ansatz. Here, by following previous works [15–17], we consider the parameter-dependent ansatz

$$v(x, y, t; \eta, a, E) = \sqrt{\frac{\eta E}{2\pi a^2}}\,\text{sech}(\eta t)\exp\left(-\frac{x^2 + y^2}{2a^2}\right), \quad (8)$$

where a is the width of the spatial Gaussian profile, η^{-1} is the temporal width, and E is the STS energy.

With this ansatz, the Lagrangian of the system

$$L \equiv \int_{\mathbb{R}^3}\mathcal{L}_v(v, v_{tt}, v_x, v_y)dxdydt \quad (9)$$

reduces to

$$L = \frac{E}{30}\left[-14d_4\eta^4 - 30\kappa + \frac{5}{a^2}\left(\frac{E\eta\nu}{2\pi} - 3\right) + 15\rho a^2\right], \quad (10)$$

which possesses all relevant information for approximate solutions of the form (8). For Eq. (10), the reduced Euler-Lagrange equations for the parameters a, η, and E read as

$$\frac{\partial L}{\partial\eta} = 0, \qquad \frac{\partial L}{\partial a} = 0, \qquad \frac{\partial L}{\partial E} = 0, \quad (11)$$

which lead, respectively, to the following equations:

$$\frac{5\nu E}{\pi a^2} - 112d_4\eta^3 = 0 \quad (12a)$$

$$\eta = \frac{6\pi(a^4\rho + 1)}{\nu E} \quad (12b)$$

$$\kappa = -\frac{7}{15}d_4\eta^4 - \frac{1}{2a^2}\left(1 - \frac{E\eta\nu}{3\pi}\right) + \frac{\rho a^2}{2}. \quad (12c)$$

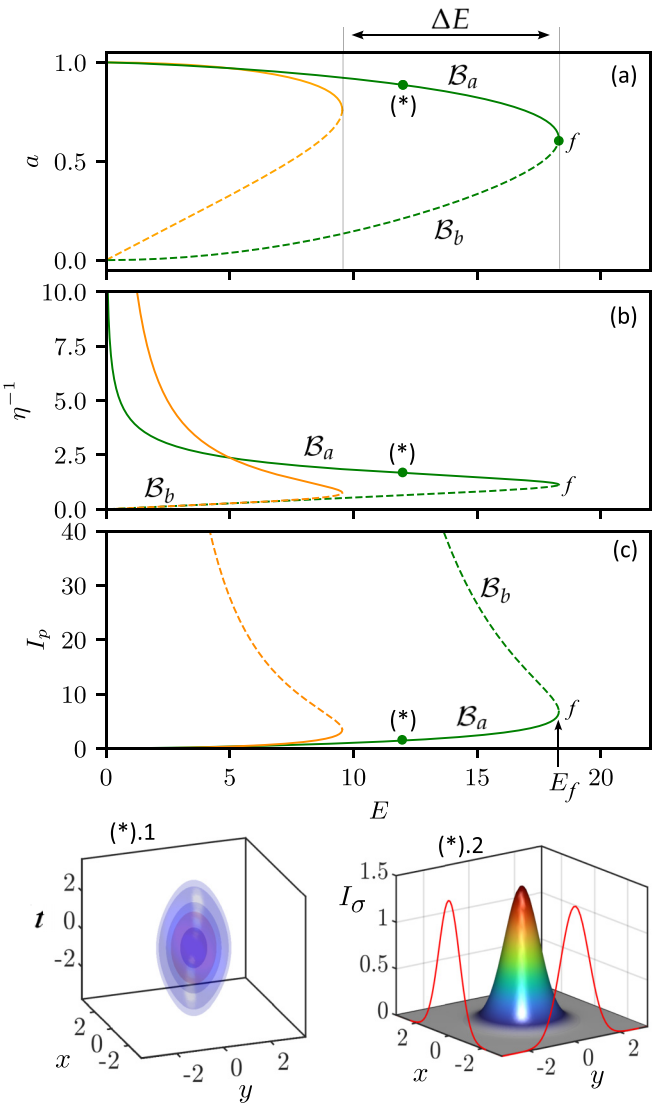

FIG. 1. Bifurcation diagrams for STS states vs E (see green lines). (a) Spatial width a of the STS vs E. (b) STS temporal width η^{-1} vs. E, and (c) variation of the peak intensity I_p with E. The $\mathcal{B}_a$ branch of solutions is plotted by using a solid line, while $\mathcal{B}_b$ uses a dashed one. Orange lines correspond to the pure quadratic scenario [17]. Label (*) corresponds to the STS depicted in panels (*).1 and (*).2. In (*).1 we plot five isosurfaces at different peak intensities, namely, $I = 0.08, 0.12.0.3, 0.5$, and 1.0. Panel (*).2 illustrates the $t = 0$ cross-section intensity $I_\sigma \equiv I(x, y, t = 0)$ for the STSs shown above.

By combining Eqs. (12a) and (12b), we obtain

$$E^4 = C_1 d_4 \pi^4 a^2 (a^4 \rho + 1)^3, \tag{13}$$

with $C_1 = 1008 \times 24/5$, which relates E and a. By inserting Eq. (13) into Eq. (12b), we find that the temporal width η^{-1} is also completely parametrized in terms of the spatial width a.

In what follows, we will focus on the regime that is characterized by setting $d_4 = 1$, $\rho = -1$, and $\nu = 1$. In this case, the dependence of the STS spatial width a on E is depicted in Fig. 1(a). This plot shows that there exist two STS solution branches $\mathcal{B}_a$ (solid green) and $\mathcal{B}_b$ (dashed green), which coexist within the same energy range, extending from $E = 0$ up to

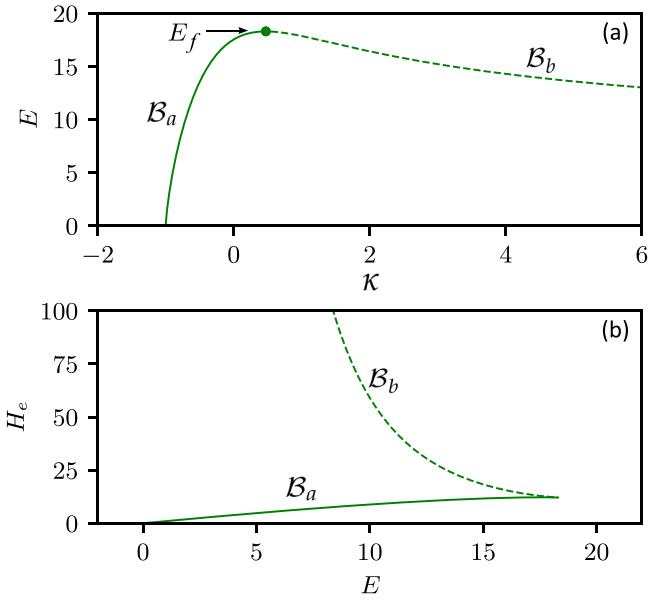

FIG. 2. (a) Dependence of energy E with κ for $\rho = -1$ and $\nu = d_4 = 1$. (b) Dependence of H with E. In both cases, stable (unstable) branches are plotted by using solid (dashed) lines.

the fold (f) located at $(E, a) = (E_f, a_f)$. The position of this fold can be computed from the condition $dE/da = 0$, which yields

$$a_f = (-7\rho)^{-1/4} \qquad E_f^4 = C_2 \frac{\pi^4 d_4}{\sqrt{-7\rho}}, \tag{14}$$

with $C_2 = C_1(6/7)^3$, and marks an upper energy limit, or threshold, for the STS existence. The modifications of the temporal width and the STS peak intensity $I_p \equiv |A|^2 = E\eta/(2\pi a^2)$ with energy E are illustrated in Figs. 1(b) and 1(c), respectively. A specific example of STS solution on the branch $\mathcal{B}_a$ is shown in Fig. 1(*) for $E = 12$. In Figs. 1(a)–1(c) we also plot, in orange, the STS solution branches for the pure quadratic dispersion regime [17]. The comparison between these curves shows that the STS existence region for pure quartic dispersion is $\Delta E \approx 8.753$ larger than in the quadratic case [see Fig. 1(a)].

In order to determine the stability of the STS states, we apply two different approaches. The first, known as the Vakhitov-Kolokov (VK) criterion [39], is based on the dependence of the propagation constant κ on E [see Eq. (12c)], which is depicted in Fig. 2(a). According to the VK principle, STS solutions are expected to be stable if E increases with κ (i.e., if $dE/d\kappa > 0$), and unstable otherwise. This means that $\mathcal{B}_a$ is stable, while $\mathcal{B}_b$ is unstable.

We can also determine the STSs stability by analyzing their Hamiltonian function

$$H = E\left[-\frac{a^2}{2}\rho + \frac{1}{2a^2}\left(1 - \frac{E\nu\eta}{6\pi}\right) + \frac{7}{15}d_4\eta^4\right]. \tag{15}$$

Once evaluated at the equilibrium STS solutions of Eqs. (12a) and (12b), the Hamiltonian becomes just a function of E, and we may write $H_e \equiv H(E)$. This function is plotted in Fig. 2(b). According to the Lyapunov stability criteria [17], all STS solutions on the $\mathcal{B}_a$ branch minimize H_e; therefore,

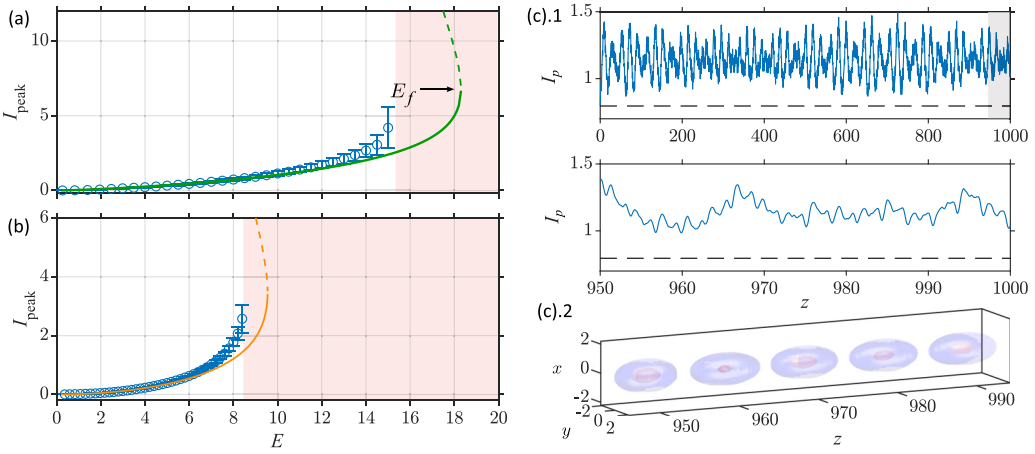

FIG. 3. (a) and (b) Evolution of peak intensity of stable STS with energy E for the pure quartic and quadratic dispersion scenarios, respectively. In (a), the green line shows the analytical values, while the blue circles and the error bars represent the average intensity values, and the standard deviation for stable states. (c).1 shows the variation of the peak STS intensity vs z, and the close-up view below shows the interval $z \in [950, 1000]$ (see gray shadowed box). (c).2 shows the evolution of the STS along the latter interval, by plotting two isosurfaces at $I_1 = 0.5$ (red) and $I_2 = 0.1$ (blue).

they are stable. However, those on $\mathcal{B}_b$ are unstable, since they maximize H_e. Thus, both stability criteria lead to the same result.

IV. NUMERICAL STUDY

The question that remains to be answered is whether such approximate solutions, and their predicted stability, describe accurately enough the STS solutions of Eq. (2). To bring light to this, we performed full 3D numerical simulations of Eq. (2) by using advanced numerical algorithms based on a split-step predictor-corrector scheme [40]. To solve this initial value problem, we consider as the initial condition the approximate analytical STS solution (8), together with Eqs. (12a) and (12b). The outcome of these computations is illustrated in Fig. 3. Figure 3(a) compares the analytically predicted peak intensity of the STS (see green line) with the numerically obtained associated values (see blue dots). In the latter, the circles and error bars represent the time-averaged intensity values, and the corresponding standard deviation for stable states. Stable STS are center steady states of Eq. (2) [17]: Therefore, they are neutrally stable. This means that any small perturbation leads to breathing oscillations around such points. Therefore, in practice, a steadily propagating STS is difficult to achieve. This fact may explain why, while the agreement between the variational approach and numerical results is quite good for low values of energy, it worsens when increasing E. The z propagation of a STS is illustrated in Fig. 3(c).2, together with the z evolution of its peak intensity [see Fig. 3(c).1] for the interval $z \in [0, 1000]$. Larger simulations (up to a final normalized propagation distance $z_f = 5000$) have confirmed the robustness of these states.

For large values of E, we find that the STSs undergo wave collapse (see red shadowed area) before the fold f, as was the case in the pure quadratic regime [17]. To compare the latter scenario with the former one, we plot approximate and numerically obtained I_p values for pure quadratic dispersion in Fig. 3(b). This comparison shows that pure quartic dispersion significantly delays the appearance of wave collapse, by increasing by more than twice the E range of STS existence.

V. CONCLUSIONS

In this work we have reported on the emergence of pure quartic STSs in GRIN waveguides. We show that pure positive quartic dispersion affects undoubtedly the propagation of STS, by leading to a significant widening of their energy stability range, and to the partial arrest of spatiotemporal collapse.

In the absence of the GRIN structure, positive quartic and anomalous quadratic dispersion are also capable of arresting spatiotemporal wave collapse; however, this is insufficient for prompting the formation of STSs [32,33]. In contrast, even a small amount of negative quartic dispersion may lead to the appearance of light bullets in both homogeneous planar waveguides and bulk media, something that we have not investigated in the present work.

One potential experimental scheme where our results may apply can be based on the experimental setup of de Sterke *et al.* [31], by changing the single-mode fiber to a multimode GRIN one. Indeed, our model [see Eq. (1)] is the master equation describing such a fiber laser when losses and gain are equally balanced. For some physical parameter values regarding our model in the context of multimode GRIN fibers, we invite the interested reader to consult Ref. [37].

In future investigations, we will analyze the implications of combining quadratic and quartic dispersion effects, as well as the influence of higher-order diffraction on STS stabilization, which so far remain unknown. Another potential line of research is related to the interaction of STSs and the excitation of high-order states, such as the dipole STSs shown in Ref. [41].

ACKNOWLEDGMENTS

This work was supported by Marie Sklodowska-Curie Actions (Grants No. 101023717 and No. 101064614), the

Sapienza University Grants AddSapiExcellence (NOSTER-DIS) and the Additional Activity for MSCA (EFFILOCKER), the European Union under the Italian National Recovery and Resilience Plan (NRRP) NextGenerationEU, partnership on "Telecommunications of the Future" (PE00000001–program "RESTART").

[1] Y. S. Kivshar, G. P. Agrawal, and Y. S. Kivshar, *Optical Solitons: From Fibers to Photonic Crystals* (Academic Press, New York, 2003).

[2] Y. V. Kartashov, G. E. Astrakharchik, B. A. Malomed, and L. Torner, Frontiers in multidimensional self-trapping of nonlinear fields and matter, Nat. Rev. Phys. **1**, 185 (2019).

[3] B. A. Malomed, *Multidimensional Solitons* (AIP Publishing, Melville, 2022).

[4] Y. Silberberg, Collapse of optical pulses, Opt. Lett. **15**, 1282 (1990).

[5] S. Minardi, F. Eilenberger, Y. V. Kartashov, A. Szameit, U. Röpke, J. Kobelke, K. Schuster, H. Bartelt, S. Nolte, L. Torner, F. Lederer, A. Tünnermann, and T. Pertsch, Three-dimensional light bullets in arrays of waveguides, Phys. Rev. Lett. **105**, 263901 (2010).

[6] W. H. Renninger and F. W. Wise, Optical solitons in graded-index multimode fibres, Nat. Commun. **4**, 1719 (2013).

[7] P. Panagiotopoulos, P. Whalen, M. Kolesik, and J. V. Moloney, Super high power mid-infrared femtosecond light bullet, Nat. Photon. **9**, 543 (2015).

[8] L. Bergé, Wave collapse in physics: Principles and applications to light and plasma waves, Phys. Rep. **303**, 259 (1998).

[9] O. Bang, W. Krolikowski, J. Wyller, and J. J. Rasmussen, Collapse arrest and soliton stabilization in nonlocal nonlinear media, Phys. Rev. E **66**, 046619 (2002).

[10] W. Krolikowski, O. Bang, J. J. Rasmussen, and J. Wyller, Modulational instability in nonlocal nonlinear Kerr media, Phys. Rev. E **64**, 016612 (2001).

[11] F. Dohmen, J. Javaloyes, and S. V. Gurevich, Bound states of light bullets in passively mode-locked semiconductor lasers, Chaos **30**, 063120 (2020).

[12] J. Javaloyes, Cavity light bullets in passively mode-locked semiconductor lasers, Phys. Rev. Lett. **116**, 043901 (2016).

[13] S. S. Gopalakrishnan, K. Panajotov, M. Taki, and M. Tlidi, Dissipative light bullets in Kerr cavities: Multistability, clustering, and rogue waves, Phys. Rev. Lett. **126**, 153902 (2021).

[14] P. Horak and F. Poletti, Multimode nonlinear fibre optics: Theory and applications, in *Recent Progress in Optical Fiber Research*, edited by M. Yasin, S. W. Harun, and H. Arun (Intechopen, Rijeka 2012).

[15] S.-S. Yu, C.-H. Chien, Y. Lai, and J. Wang, Spatio-temporal solitary pulses in graded-index materials with Kerr nonlinearity, Opt. Commun. **119**, 167 (1995).

[16] S. Raghavan and G. P. Agrawal, Spatiotemporal solitons in inhomogeneous nonlinear media, Opt. Commun. **180**, 377 (2000).

[17] P. Parra-Rivas, Y. Sun, and S. Wabnitz, (Invited) Spatiotemporal soliton stability in multimode fibers: A Hamiltonian approach, Optik **287**, 171079 (2023).

[18] C. Milián and D. V. Skryabin, Soliton families and resonant radiation in a micro-ring resonator near zero group-velocity dispersion, Opt. Express **22**, 3732 (2014).

[19] P. Parra-Rivas, D. Gomila, F. Leo, S. Coen, and L. Gelens, Third-order chromatic dispersion stabilizes Kerr frequency combs, Opt. Lett. **39**, 2971 (2014).

[20] P. Parra-Rivas, D. Gomila, and L. Gelens, Coexistence of stable dark- and bright-soliton Kerr combs in normal-dispersion resonators, Phys. Rev. A **95**, 053863 (2017).

[21] M. Tlidi and L. Gelens, High-order dispersion stabilizes dark dissipative solitons in all-fiber cavities, Opt. Lett. **35**, 306 (2010).

[22] H. Taheri and A. B. Matsko, Quartic dissipative solitons in optical Kerr cavities, Opt. Lett. **44**, 3086 (2019).

[23] P. Parra-Rivas, S. Hetzel, Y. V. Kartashov, P. F. de Córdoba, J. A. Conejero, A. Aceves, and C. Milián, Quartic Kerr cavity combs: Bright and dark solitons, Opt. Lett. **47**, 2438 (2022).

[24] A. F. J. Runge, D. D. Hudson, K. K. Tam, C. M. de Sterke, and A. Blanco-Redondo, The pure-quartic soliton laser, Nat. Photon. **14**, 492 (2020).

[25] M. Karlsson and A. Höök, Soliton-like pulses governed by fourth order dispersion in optical fibers, Opt. Commun. **104**, 303 (1994).

[26] N. N. Akhmediev, A. V. Buryak, and M. Karlsson, Radiationless optical solitons with oscillating tails, Opt. Commun. **110**, 540 (1994).

[27] S. Roy and F. Biancalana, Formation of quartic solitons and a localized continuum in silicon-based slot waveguides, Phys. Rev. A **87**, 025801 (2013).

[28] K. K. K. Tam, T. J. Alexander, A. Blanco-Redondo, and C. M. de Sterke, Stationary and dynamical properties of pure-quartic solitons, Opt. Lett. **44**, 3306 (2019).

[29] A. Höök and M. Karlsson, Ultrashort solitons at the minimum-dispersion wavelength: Effects of fourth-order dispersion, Opt. Lett. **18**, 1388 (1993).

[30] A. Blanco-Redondo, C. M. de Sterke, J. E. Sipe, T. F. Krauss, B. J. Eggleton, and C. Husko, Pure-quartic solitons, Nat. Commun. **7**, 10427 (2016).

[31] C. M. de Sterke, A. F. J. Runge, D. D. Hudson, and A. Blanco-Redondo, Pure-quartic solitons and their generalizations—theory and experiments, APL Photon. **6**, 091101 (2021).

[32] G. Fibich, B. Ilan, and S. Schochet, Critical exponents and collapse of nonlinear Schrödinger equations with anisotropic fourth-order dispersion, Nonlinearity **16**, 1809 (2003).

[33] G. Fibich and B. Ilan, Optical light bullets in a pure Kerr medium, Opt. Lett. **29**, 887 (2004).

[34] V. M. Pérez-García, H. Michinel, J. I. Cirac, M. Lewenstein, and P. Zoller, Dynamics of Bose-Einstein condensates: Variational solutions of the Gross-Pitaevskii equations, Phys. Rev. A **56**, 1424 (1997).

[35] B. A. Malomed, Variational methods in nonlinear fiber optics and related fields, in *Progress in Optics* (Elsevier, New York, 2002), Vol. 43, pp. 71–193.

[36] G. P. Agrawal, *Physics and Engineering of Graded-Index Media* (Cambridge University Press, Cambridge, UK, 2023).

[37] Y. Sun, P. Parra-Rivas, M. Zitelli, F. Mangini, M. Ferraro, and S. Wabnitz, 2 - An introduction to guided-wave nonlinear ultrafast photonics, in *Advances in Nonlinear Photonics*, edited by G. C. Righini and L. Sirleto, Woodhead Publishing Series in Electronic and Optical Materials (Woodhead Publishing, Cambridge, 2023), pp. 27–55.

[38] R. Abraham and J. E. Marsden, *Foundations of Mechanics* (American Mathematical Society, Providence, 2008).

[39] N. G. Vakhitov and A. A. Kolokolov, Stationary solutions of the wave equation in a medium with nonlinearity saturation, Radiophys. Quantum Electron. **16**, 783 (1973).

[40] P. Frolkovič, Numerical recipes: The art of scientific computing, Acta Appl. Math. **19**, 297 (1990).

[41] O. V. Shtyrina, M. P. Fedoruk, Y. S. Kivshar, and S. K. Turitsyn, Coexistence of collapse and stable spatiotemporal solitons in multimode fibers, Phys. Rev. A **97**, 013841 (2018).